Journal of Nuclear Materials 395 (2009) 11–22

Contents lists available at ScienceDirect

Journal of Nuclear Materials

journal homepage: www.elsevier.com/locate/jnucmat

Irradiation-assisted stress corrosion cracking of austenitic alloys in supercritical water

Rongsheng Zhou, Elaine A. West, Zhijie Jiao, Gary S. Was *

Department of Nuclear Engineering and Radiological Sciences, University of Michigan, 2355 Bonisteel Boulevard, Ann Arbor, MI 48109, United States

ARTICLE INFO

Article history:
Received 9 July 2009
Accepted 23 September 2009

ABSTRACT

Four commercial austenitic alloys, 316L, D9, 690 and 800H were irradiated with 2.0 MeV protons to doses of up to 7 dpa at temperatures of 400 and 500 °C to study the role of irradiation and temperature on stress corrosion cracking in supercritical water. Constant extension rate tensile (CERT) tests were performed on the irradiated specimens in deaerated supercritical water at the same temperature as the irradiation. The results showed that irradiation significantly increased the severity of intergranular stress corrosion cracking in all four alloys. Cracking severity increased with dose and temperature. The severity of cracking correlated with both the hardness and the grain boundary chromium concentration, making attribution to a single irradiation feature difficult. However, a very significant increase in cracking of alloy 690 at 500 °C is likely due primarily to RIS rather than to hardening. Cracking of the irradiated alloys in supercritical water follows the same behavior as in subcritical water, implying that a common mechanism may be controlling.

1. Introduction

The supercritical water cooled reactor (SCWR) is one of the promising Generation IV advanced reactor concepts with a high thermal efficiency (~45%) and considerable plant simplification compared to current light water reactors (LWRs) [1]. The SCWR concept, with an inlet temperature of ~280 °C and an outlet temperature of up to 620 °C and system pressure of 25 MPa, builds upon two existing technologies, LWRs and supercritical fossil fuel plants. The combination of radiation, high temperatures, high pressures and a corrosive water environment makes the SCWR one of the most challenging reactors from the standpoint of materials selection. Therefore, the core internal materials for SCWR are required to have sufficient mechanical properties, corrosion resistance, low susceptibility to SCC, reasonably low neutron absorption and dimensional stability in the SCWR environment.

Candidate materials for core internals for the SCWR include ferritic–martensitic (F–M) stainless steels (including ODS alloys) and austenitic alloys (including austenitic stainless steels and nickel-base alloys). F–M alloys such as T91 and HT9 are candidate structural materials for SCWR because of their wide use in supercritical fossil plants. Was et al. [2,3] evaluated T91, T92, HCM12A and HT9 in 400–600 °C SCW and they were shown to be resistant to SCC in a SCW environment, but their high corrosion rates prohibit their use in thin wall components such as fuel cladding. Austenitic alloys are candidate materials for the SCWR because of their high corrosion resistance and good mechanical properties at high temperatures and their experience base in current commercial light water reactors. Teysseyre and Was [4,5] evaluated the corrosion and stress corrosion cracking susceptibility in supercritical water and found that while general corrosion rates are low, all alloys were susceptible to intergranular SCC (IGSCC) in both deaerated and oxygen-containing supercritical water.

An understanding of the effect of irradiation on SCC or irradiation-assisted stress corrosion cracking (IASCC) is more limited still. In this study, the IASCC behavior of four commercial austenitic alloys 316L, D9, 800H and 690 in pure SCW was investigated at temperatures of 400 and 500 °C and at doses between 2 and 7 dpa. The effect of irradiation on the microstructure is also characterized and the microstructure development is used to understand the mechanism of IASCC.

2. Experiment

2.1. Alloy and sample preparation

Four commercial purity austenitic alloys were evaluated in this study: Stainless steels 316L and D9, high nickel austenitic alloy 800H, and nickel-base alloy 690. The compositions of the alloys are shown in Table 1. The as-received 316L alloy was annealed at 1100 °C for 20 min and water quenched to prevent carbide

* Corresponding author. Tel.: +1 734 763 4675; fax: +1 734 763 4540.
E-mail address: gsw@umich.edu (G.S. Was).

0022-3115/$ - see front matter © 2009 Elsevier B.V. All rights reserved.
doi:10.1016/j.jnucmat.2009.09.010

Table 1
Alloy compositions (wt.%).

Alloy	C	Mn	Fe	S	Si	Ni	Cr	Mo	Cu	N	Co	P	Al	Ti	Nb
316L	0.022	1.86	68.5	0.001	0.51	10.12	16.62	2.06	0.24	0.02	0.05	0.03	–	–	–
D9	0.043	2.03	65.7	<0.005	0.66	15.12	13.95	2.2	0.005	–	0.014	<0.005	0.014	0.26	<0.02
690	0.03	0.18	10	0.001	0.03	59.8	29.4	0.01	0.01	–	–	–	0.22	0.34	<0.01
800H	0.069	0.76	45.26	0.001	0.13	31.59	20.42	–	0.42	–	–	0.014	0.5	0.57	–

formation, and resulted in a grain size of 44 μm. Alloy 690 was cold-rolled to 66% reduction and then annealed at 1100 °C for 2 h in order to obtain a uniform grain size of 28 μm. D9 was cold-worked to 18% and the grain size was 17 μm. Alloy 800H was evaluated in the as-received condition and had a grain size of 152 μm and extensive chromium carbide precipitation on the grain boundaries.

Tensile specimens with threaded ends, gage cross-section of 2 mm × 2 mm and a gage length of 23 mm, and TEM bars with dimensions of 20 mm × 2 mm × 2 mm were fabricated using electrical discharge machining. The irradiated TEM bars were used to measure irradiation hardening and to make TEM discs for microstructure and RIS analysis. All specimens were mechanically polished with SiC paper to 4000 grit and then electropolished in a 10% perchloric and methanol solution at 30 V for 15 s to achieve mirror surfaces. The D9 and 316L specimens were electropolished at −50 °C and the 800H and 690 were electropolished at −30 °C. Following sample preparation, hardness measurements were made on each TEM bar.

2.2. Proton irradiation

The TEM and tensile specimens were irradiated using the General Ionex Tandetron Accelerator at the Michigan Ion Beam Laboratory at the University of Michigan. The samples were loaded onto a custom designed copper stage and irradiated with 2 MeV protons at 400 or 500 °C to doses ranging from 2 to 7 dpa at a dose rate of 10^{-5} dpa/s. Some samples were irradiated at 3 MeV. The damage rate was estimated by performing a SRIM2006 simulation [6] using a displacement energy of 40 eV as recommended in ASTM E521-89 [7]. A plot of the damage distribution of 2 and 3 MeV protons in Fe–10Cr is shown in Fig. 1.

The temperature was controlled to ±10 °C with a cartridge heater and by cooling the back of the copper stage. Thermal contact between the specimens and the stage was achieved by placing thin sheets of indium foil beneath the samples, which became molten at the irradiation temperature to provide good heat transfer. The temperature of the specimens was monitored using a high spatial resolution two-dimensional thermal imaging system and provided a complete time history of the temperatures of each region of each sample. Fig. 2 shows the temperature histogram for one of the samples irradiated to 7 dpa.

The proton beam was 3 mm in diameter and was raster-scanned over a 10 mm length of the specimens. The irradiated area

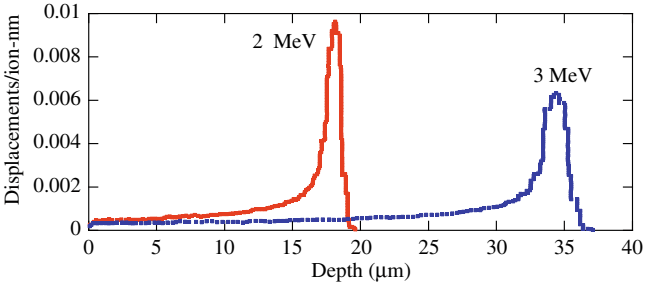

Fig. 1. SRIM plot for 2 and 3 MeV protons in Fe–10Cr.

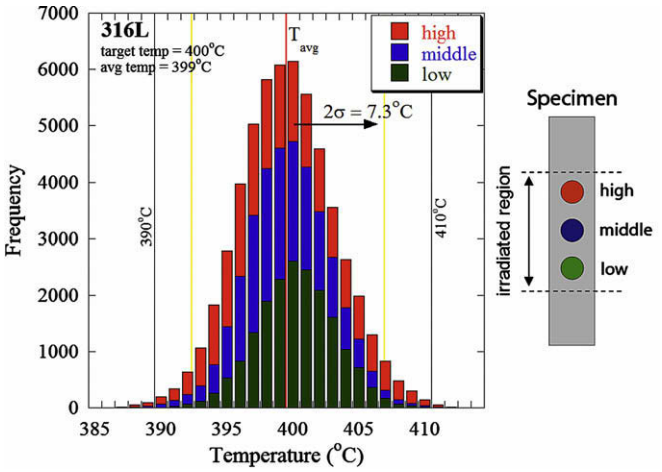

Fig. 2. Histogram of an irradiation of 316L to a dose of 7 dpa at 400 °C.

of the samples was defined by a set of tantalum apertures and approximately 8 samples were irradiated at one time. The temperatures, stage current, and aperture current were recorded throughout the test using a PC-based monitoring system. Additional details about the proton irradiation procedure can be found in other literature [8].

2.3. Hardness measurement and microstructure analysis

The pre-irradiation and post-irradiation hardness of the specimens was determined using a Vickers Microhardness tester (Micromet-II). A 25 g load was used to ensure that the sampling volume of the indenter tip was confined to the irradiated region of the material. A total of 30 hardness measurements were made on each specimen, and the center-to-center spacing of the indents was 100 μm. The difference between the post-irradiation and pre-irradiation hardness is reported as the irradiation-induced hardening. The results of these measurements were compared to the unirradiated hardness values for each sample. The pre- and post-irradiation hardness values were used to calculate the radiation-induced hardening increment.

A correlation between the change in yield strength and change in hardness of austenitic alloys was provided by Busby et al. [9] and was used to determine the change in yield stress in MPa in all three alloys according to:

$$\Delta\sigma_y = 3.03 \times \Delta H, \tag{1}$$

where $\Delta\sigma_y$ is in MPa and ΔH is in kg/mm^2. The change in yield strength can also be calculated using the loop and void measurements made on the irradiated microstructure from [10]:

$$\Delta\sigma_y = M\alpha\mu b(\mathrm{Nd})^{0.5}, \tag{2}$$

where $M = 3.06$, $\alpha = 1.0$ for voids and 0.6 for faulted loops (determined from a regression analysis), $\mu = 76$ GPa, and $b = 2.5 \times 10^{-8}$ cm. The total change in yield strength from the loop and void

contributions is equal to the square root of the sum of the squares of each individually:

$$\Delta\sigma_{total} = (\Delta\sigma^2_{loop} + \Delta\sigma^2_{void})^{0.5}. \quad (3)$$

The irradiated microstructures of the alloys were analyzed using TEM discs made from the TEM bars. Each TEM bar yielded five discs; three discs from the irradiated region of the bar and two discs from the unirradiated ends of the bar. The bars were reduced to 100 μm thickness by mechanically polishing from the unirradiated side. A 3 mm diameter slurry cutter was used to cut out the discs. The discs were then electropolished from the irradiated surface for ~7 s in a 5% perchloric acid and 95% methanol solution at −50 °C using a single jet thinner. The final TEM foils were obtained by jet-thinning from the unirradiated surface in the same solution until perforation occurred.

The analysis of the irradiation-induced microstructure was performed using the JEOL 2010F analytical TEM at the University of Michigan Electron Microbeam Analysis Laboratory. The irradiation-induced faulted dislocation loops were analyzed using the rel-rod technique [11]. The sample was rotated near the [0 1 1] beam direction and rel-rod dark field images of the loops were collected. The average loop diameter was determined from the average of over 400 loop/diameter measurements. The loop density was measured by dividing the total number of loops per unit area by the thickness of the TEM specimen in the area where the rel-rod image was recorded. The best images of the irradiation-induced voids were obtained in a slightly underfocused condition. Elemental segregation at the grain boundaries was measured via STEM/EDS. The grain boundary was aligned edge-onto the electron beam, and a probe size of 0.5 nm was used to measure the grain boundary composition profile in 1.0 nm steps along a 30 nm line scan perpendicular to the boundary. Composition measurements were taken over a period of 20–30 s to minimize the error due to drift, and multiple measurements were taken at each boundary. In order to ensure accurate measurements at the grain boundaries for the 316L and 690 specimens, approximately five additional spot measurements were taken at the exact boundary location.

2.4. Stress corrosion cracking experiments

Stress corrosion cracking susceptibility was determined via constant extension rate tensile (CERT) tests performed in a closed flowing water loop. The CERT tests were performed in a 4 liter autoclave made of nickel-base alloy 625. Water was circulated through the system using a high-pressure liquid chromatography (HPLC) pump at a flow rate of 40–50 ml/min. The temperature was maintained at 400 °C or 500 °C using a convection preheater system and by adjusting the temperature of the heater bands located on the outside of the autoclave. The pressure was controlled with a back pressure regulator. The water was circulated through an ion exchange column to maintain a conductivity of below 0.1 μS/cm, and the dissolved oxygen content of the water was measured at less than 10 ppb by flowing argon through the water column. Four irradiated specimens were strained simultaneously to failure in deaerated SCW at 400 or at 500 °C at a pressure of 24 MPa. Straining did not commence until the temperature, pressure, and water purity stabilized, which required approximately 14 h. Samples were strained at a rate of 3×10^{-7} s^{-1} using a stepping motor.

Following test completion, the specimens were examined using a JOEL JSM-6480 scanning electron microscope (SEM). The unirradiated data were collected from the unirradiated gage surfaces of the irradiated specimens, while the irradiated data were collected on the 10 mm length of the specimen that had been irradiated. Gage surface analysis was confined to a region of nearly uniform crack density that did not include areas in the necked region of the specimen or areas far from the fracture point. Images of the gage surfaces taken at 250× were used to determine the crack density and average crack length. The crack length per unit area was also determined by dividing the sum of the crack lengths by the area of the specimen that was analyzed. This measurement accounts for both the crack length and density and so it was regarded as the best indication of the IGSCC susceptibility of the alloy. Crack depth measurements were made by mounting the tensile specimens in epoxy and polishing away a portion of the gage surface to reveal the sample cross-section. The maximum crack depth into the irradiated and unirradiated surfaces was determined from the recorded SEM images. The fracture surfaces of the specimens were also analyzed to determine the %IG fracture. Analysis was performed independently on the unirradiated and the 20 μm thick irradiated portion of the surface.

3. Results

Results are presented on the effect of irradiation on the microstructure (loops, voids), irradiation hardening, radiation-induced segregation, and stress corrosion cracking. Stress corrosion cracking is characterized by the number of cracks per unit area, the crack depth in the gage section and the %IG on the fracture surface.

3.1. Irradiated microstructure

Fig. 3 shows dark-field micrographs of samples of 316L and 690 irradiated to 2 and 7 dpa at 400 °C and to 7 dpa at 500 °C. The loop size distributions for these conditions were determined from measurements of edge-on loops in rel-rod dark field images and are summarized in Table 2. Fig. 4a and b shows the loop size distribution for 316L and 690, respectively. In the 316L case, the distribution changes very little between 2 and 7 dpa at 400 °C, but the distribution shifts to larger size for the irradiation at 500 °C. For 690, the loop size distribution following irradiation at 400 °C to 7 dpa has a longer tail than that at 2 dpa. Irradiation at 500 °C results in a shift of the curve to higher loop sizes as expected. The average loop size and loop number density for both alloys are shown in Fig. 5. Note that the changes in loop size and number density with dose are comparable between the two alloys. As dose increases from 2 to 7 dpa for 316L at 400 °C, the dislocation loop size decreases slightly but the dislocation loop density increases by more than a factor of two. For alloy 690 at 400 °C, the dislocation loop size increases slightly and the dislocation loop density increases by more than a factor of 4. As temperature increases from 400 to 500 °C at 7 dpa, the mean dislocation loop size in both 316L and 690 increases, but the extent of the increase is greater in 316L than in 690 alloy. The number density of dislocation loops decreases significantly with temperature in both alloys.

Bright field images of voids in 316L and 690 following irradiation to 2 and 7 dpa at 400 °C, and to 7 dpa at 500 °C are shown in Fig. 6. The void microstructure follows similar trends as shown by the plot of mean void size and number density in Fig. 7. An increase in dose from 2 to 7 dpa at 400 °C resulted in small increases in void size and more significant increases (factors of 2–4) in void number density. An increase in temperature from 400 to 500 °C resulted in a small increase in the void size in 690 (20%) and a larger increase in 316L (75%). The void number density decreases by a factor of 3 in 690 and by a factor of 6 in 316L, thus following the relative changes in the void size.

3.2. Irradiation hardening

Hardness measurements on the unirradiated specimens indicated that D9 was the hardest, followed by 690, 800H and 316L.

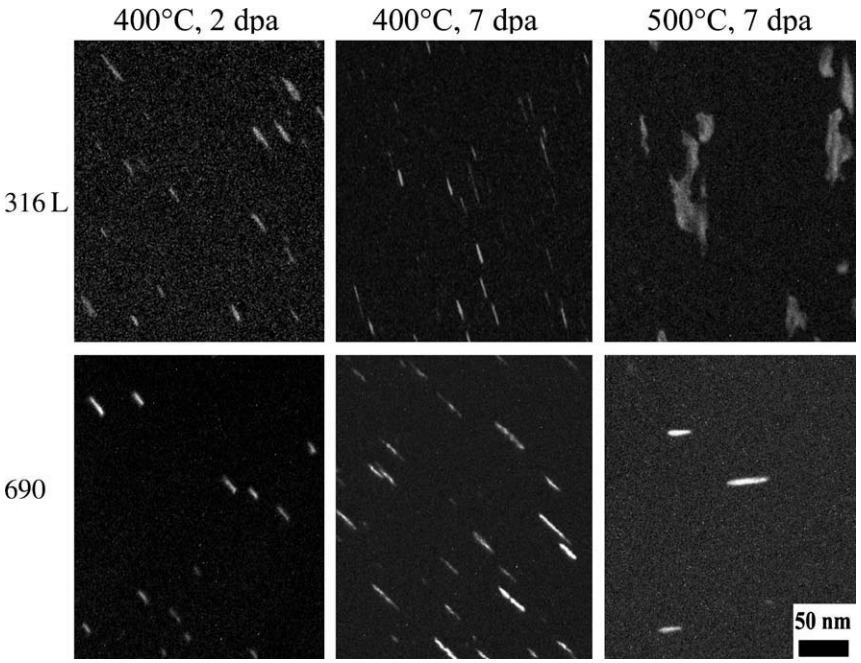

Fig. 3. Rel-rod dark field TEM images of dislocation loops in alloys 316L and 690 irradiated to 2 dpa and/or 7 dpa at 400 and 500 °C.

Table 2
Summary of dislocation loop and void measurements on specimens irradiated at 400 °C to 2 and 7 dpa and 500 °C to 7 dpa.

Alloy	Temperature (°C)	Dose (dpa)	Loops			Voids		
			# of loops measured	Mean loop diameter (nm)	Loop density (10^{21} m^{-3})	# of voids measured	Mean void size (nm)	Void density (10^{21} m^{-3})
316L	400	2	269	14.1 ± 0.3	5.74 ± 0.50	93	5.8 ± 0.2	1.63 ± 0.13
		7	247	13.5 ± 0.3	12.5 ± 1.6	206	7.7 ± 0.2	3.59 ± 0.27
	500	7	492	38.5 ± 0.9	3.14 ± 0.28	233	13.4 ± 0.1	0.59 ± 0.08
690	400	2	293	13.9 ± 0.3	3.59 ± 0.34	85	5.5 ± 0.2	0.71 ± 0.08
		7	300	17.4 ± 0.4	14.4 ± 0.4	120	5.5 ± 0.2	2.97 ± 0.59
	500	7	467	25.5 ± 1.9	0.93 ± 0.07	59	6.5 ± 0.2	1.01 ± 0.10

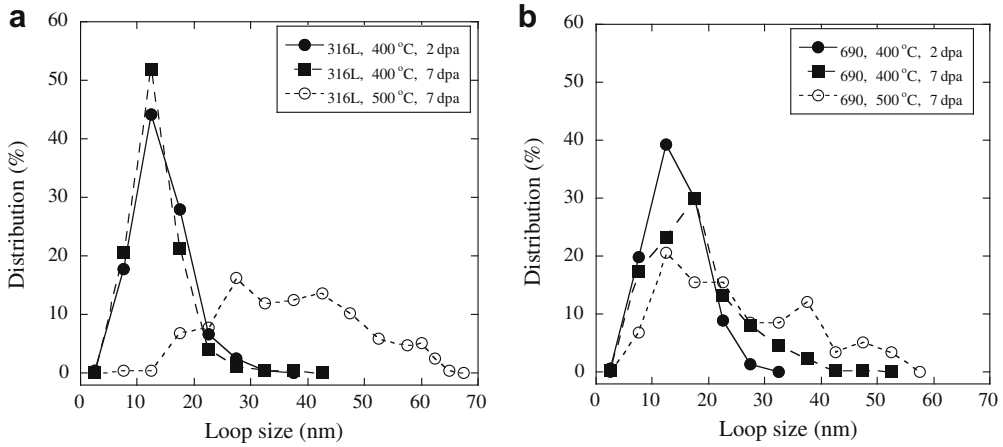

Fig. 4. Faulted loop size distributions in (a) 316L and (b) 690 following irradiation to 2 and 7 dap at 400 °C and to 7 dpa at 500 °C with 2 MeV protons.

The approximately 18% of cold-work in the processing of D9 accounted for the higher hardness in the as-received condition. Table 3 shows the results of hardness measurement for all alloys as a function of dose and temperature. Hardness increased after irradiation for all four alloys at both 400 and 500 °C, but there was considerably less hardening at 500 °C than at 400 °C. Irradiation-induced hardening increases with dose are shown in Fig. 8. With the exception of the 400 °C:4 dpa case, hardening of 316L alloy increased more than that for 690 for the same irradiation dose. By 7 dpa, the hardness of 316L and 690 have increased by 163 and

127 Hv, respectively. At 500 °C and 7 dpa, Alloys 690 and D9 had similar hardness increases of 85 and 84 Hv, respectively. The low amount of hardening of alloy D9 is likely due to the cold-worked structure of the alloy. Hardening in alloys 316L and 800H was greater at 500 °C than for D9 and 690. Overall, alloy 316L exhibited the most radiation-induced hardening followed by 800H, 690 and D9, respectively.

3.3. Radiation-induced segregation

Table 4 summarizes the RIS measurements for alloys 316L and 690 irradiated to 2 and 7 dpa. Typical composition profiles for the three main elements Fe, Cr and Ni for each irradiation condition are shown in Fig. 9. Note that as reported previously [12], both alloys began with substantial enrichment of Cr at the grain boundary, due to processing. In alloy 690, the initial grain boundary Cr concentration was over 50 wt.%. A comparison of grain boundary Cr and Ni concentration in alloys 316L and 690 as a function of dose and temperature are shown in Fig. 10. Depletion of Cr and enrichment of Ni was observed in both 316L and 690 alloys. Irradiation of alloy 316L to 2 dpa resulted in a grain boundary Cr concentration of less than 12 wt.%, compared to 19 wt.% in the unirradiated case, Fig. 10a. Nickel enriched from less than 10 wt.% to more than 18 wt.%. Very little change occurred between 2 and 7 dpa. At 500 °C, Cr depletion was slightly greater and Ni enrichment was slightly less than at 400 °C.

For alloy 690, grain boundary chromium content dropped after 2 dpa at 400 °C, but did not deplete below the bulk level until 7 dpa where it reached a value of 24 wt.% compared to the unirradiated value of 52 wt.%, Fig. 10b. Nickel enriched from 41 wt.% in the unirradiated condition to 67 wt.% after 7 dpa at 400 °C. At 500 °C:7 dpa, Cr depletion and Ni enrichment were both greater than at 400 °C. It should be noted that RIS data from the 500 °C:7 dpa condition was taken from a sample irradiated with 3 MeV protons. While little difference is expected, the results are also in line with expectations based on the dependence of RIS on temperature.

3.4. Stress corrosion cracking

CERT experiments were conducted on a total of 10 tensile specimens in deaerated SCW at temperatures of 400 and 500 °C. Three

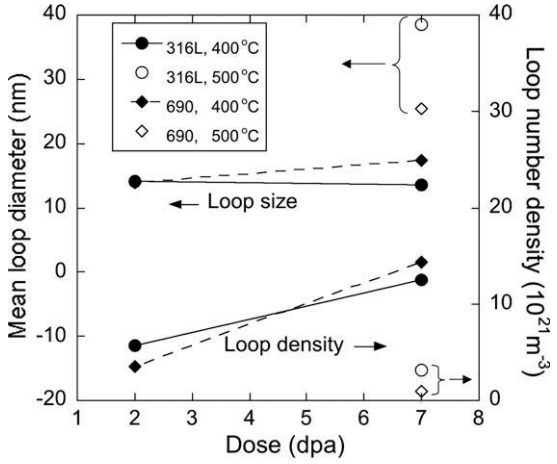

Fig. 5. Mean size and loop number density vs. dose for 316L and 690 irradiated at 400 and 500 °C.

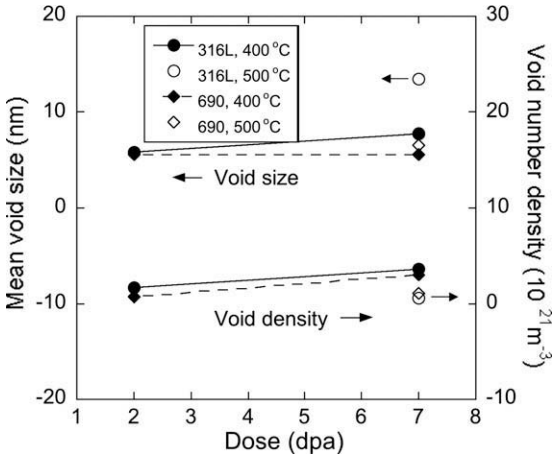

Fig. 7. Mean void and void number density vs. dose for 316L and 690 irradiated at 400 and 500 °C.

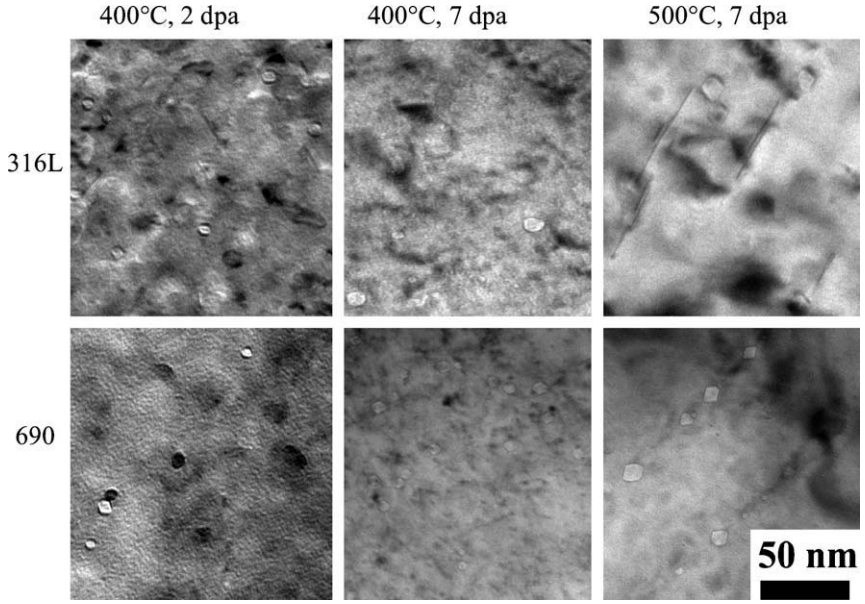

Fig. 6. TEM bright field images of voids in alloys 316L and 690 irradiated to 2 dpa and/or 7 dpa at 400 and 500 °C.

Table 3
Hardness measurements on specimens irradiated with 2 MeV protons.

Temperature (°C)	Alloy	Dose (dpa)	Unirradiated hardness		Post-irradiation hardness		Irradiation hardening		Change in yield strength (MPa)
			Measurement (Hv)	σ	Measurement (Hv)	σ	Measurement (Hv)	σ	
400	316L	2	153	5	281	12	128	13	388
		4	154	6	283	12	129	13	391
		7	152	8	315	11	163	14	494
	690	2	184	6	268	19	84	20	255
		4	181	5	327	15	146	16	442
		7	179	7	306	18	127	19	385
500	D9	7	233	12	317	20	84	23	255
	316L	7	145	10	266	17	121	20	367
	690	7	184	6	269	14	85	15	258
	800H	7	147	6	253	17	106	18	321

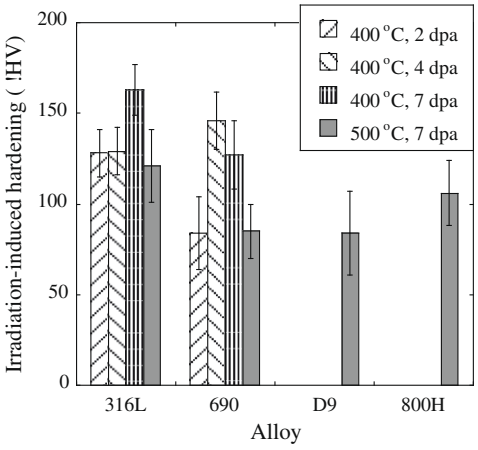

Fig. 8. Irradiation hardening for 316L, 690, D9 and 800H irradiated at 400 and 500 °C to various doses.

different measures of cracking susceptibility were used to characterize the cracking behaviors of the alloys: crack length per unit area, crack depth and percent intergranular (%IG) cracking on the fracture surface. Crack length per unit area captures both the crack density and crack length and is therefore a more complete measure of cracking on the gage surface. The crack depth is determined from cross-section analysis and %IG is determined from the fracture surface. Cracking measurement summaries of 316L, D9, 800H, 690 in SCW are shown in Table 5.

Stress–strain curves for alloy 316L irradiated to 2, 4 and 7 dpa at 400 °C and to 7 dpa at 500 °C are shown in Fig. 11 as an example of the effect of dose and temperature on the stress–strain behavior. Note that there is only minimal difference in the curves at 400 °C regardless of dose, because the irradiated depth constitutes only 1.0% of the cross-sectional area. At 500 °C, the major effect is a reduction in the strain to failure with only a small decrease in the stress. Fig. 12a and b shows the effect of dose (Fig. 12a) at 400 °C, and alloy/temperature (Fig. 12b) on the cracking as represented by the crack length per unit area. Fig. 13 shows the irradiated gage surface of 316L after straining to failure at 400 °C for several doses. Note that the cracking severity is visibly enhanced with irradiation. There is a monotonic increase in the crack length per unit area with dose for both 316L and 690 and the amount of cracking is substantially greater for 316L than for 690 by a factor of 4–5. Fig. 12b shows the alloy dependence of cracking and the temperature dependence of cracking for alloys 316L and 690. Note first that all alloys exhibit a much greater extent of cracking when irradiated to 7 dpa vs. the unirradiated case. At 400 °C, cracking in 316L is more severe than in 690, but this dependence is reversed at 500 °C. At 500 °C, the high nickel alloys (690 and 800H) exhibit greater cracking severity than the austenitic stainless steels (316L and D9). Overall, D9 exhibited the least severe cracking at 500 °C and 690 the worst.

Fig. 14a and b shows the same cracking dependences as Fig. 12a and b but using maximum crack depth as the measure of cracking severity. Fig. 14a shows that the maximum crack depth increases after the lowest dose in both 316L and 690 but remains relatively unchanged with increased dose. An increase in temperature to 500 °C resulted in an increase in the crack depth for both 316L and 690 after 7 dpa. However, the distinction between the alloys based on crack depth, Fig. 14b, is less pronounced than for the case of crack length per unit area (Fig. 12b). However, D9 still shows the least severity to cracking at both 0 and 7 dpa at 500 °C. Fig. 15 shows micrographs of cross-sections of the cracks as a function of dose for alloy 316L. Fig. 16a and b shows the cracking dependence using %IG on the fracture surface as the measure of cracking severity. Fig. 17 shows the fracture surface of a 316L sample irradiated to 7 dpa at 400 °C and strained to failure in 400 °C SCW. Note that there was no measurable IG cracking on the fracture surfaces

Table 4
STEM/EDS measurement of GB concentration in 316L and 690.

Alloy	Irradiation conditions		Cr	Fe	Ni	Si	Mo
316L	Unirradiated	Bulk	16.62	68.5	10.12	0.51	2.06
		GB	19.1 ± 1.1	63.8 ± 2.9	9.5 ± 0.5	0.8 ± 0.6	4.8 ± 1.4
	400 °C	2 dpa	11.1 ± 0.7	63.9 ± 1.4	18.3 ± 1.3	2.3 ± 0.2	3.1 ± 0.5
		7 dpa	11.7 ± 1.5	64.6 ± 1.9	18.7 ± 2.2	1.5 ± 0.3	1.8 ± 0.2
	500 °C	7 dpa	13.8 ± 1.6	53.7 ± 1.9	26.5 ± 1.0	0.8 ± 0.1	3.5 ± 0.7
690	Unirradiated	Bulk	29.4	10	59.8	NM	
		GB	52.1 ± 5.2	6.8 ± 1.2	40.7 ± 4.1		
	400 °C	2 dpa	31.7 ± 0.7	10.9 ± 1.0	57.6 ± 1.5		
		7 dpa	24.4 ± 0.5	8.8 ± 0.2	66.8 ± 0.5		
	500 °C[a]	7 dpa	15.2 ± 0.8	6.7 ± 0.8	78.1 ± 1.3		

NM = not measured.
[a] Irradiated with 3 MeV protons.

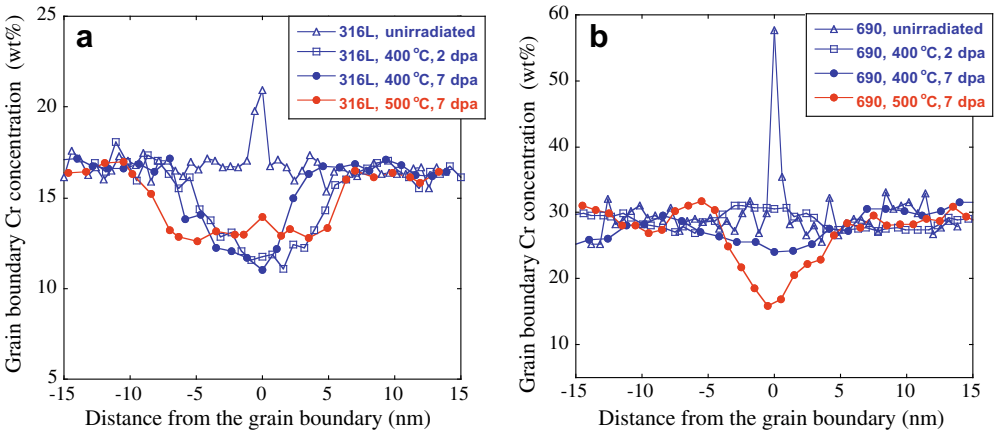

Fig. 9. Grain boundary chromium composition profiles for (a) 316L and (b) 690 following irradiation at 400 °C to 2 and 7 dpa and at 500 °C to 7 dpa.

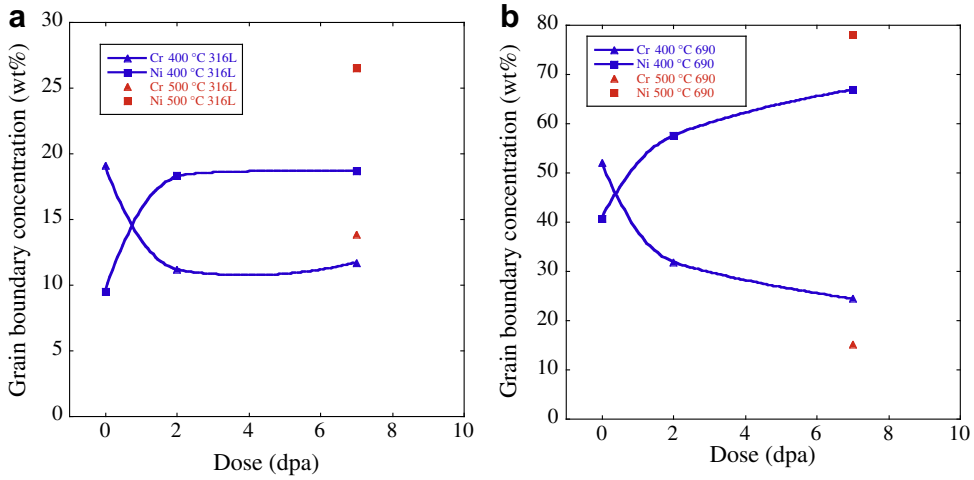

Fig. 10. Grain boundary chromium and nickel composition vs. dose for (a) 316L and (b) 690 following irradiation at 400 °C to 2 and 7 dpa and at 500 °C to 7 dpa.

at either 400 or 500 °C in the unirradiated condition. This does not mean that IG cracking did not occur, as the crack length per unit area and the crack depth analysis shows that it did occur and it was substantial. However, it is an indication that for small amounts of IG cracking with shallow penetration, %IG on the fracture surface is not a good indicator of the degree of IG cracking. This point is discussed in greater detail in Ref. [13]. Nevertheless, after 7 dpa, cracking severity at 500 °C is again the least in D9 and the greatest in 690.

4. Discussion

4.1. Alloy, dose and temperature dependence of cracking

All four alloys, 316L, D9, 690 and 800H, showed susceptibility to IGSCC in supercritical water under some conditions. In the unirradiated condition, for samples strained to failure, only alloy D9 showed no evidence of cracking by any of the measures of cracking severity (crack length per unit area, crack depth or %IG on the fracture surface). In general, cracking was most severe in 316L and 690 and less severe in 800H. At 400 °C, alloy 316L had a greater crack length per unit area than 690 at both 400 and 500 °C and crack depths were about the same. These results agree with an earlier study on the same two alloys over a range of temperatures. [4]. They are also consistent with a recent review of cracking of austenitic alloys in supercritical water [13]. Cracking in alloy 800H was evaluated only at 500 °C, and the crack length per unit area was less than for 316L and 690, but crack depth was slightly greater.

Irradiation increases cracking, regardless of alloy or temperature. The effect of irradiation on cracking is most clearly shown in Figs. 12a, 14a and 16a. Regardless of whether cracking is measured by crack length per unit area, crack depth or %IG on the fracture surface, increasing dose leads to monotonically increasing cracking by all measures. The effect of dose is greatest in the %IG cracking data shown in Fig. 16b. No observable IG cracking was found on the fracture surface in the unirradiated sample, whereas irradiation to 7 dpa led to 100%IG in 316L at 400 °C and in 690 at 500 °C. This striking difference is due to the difficulty of observing IG cracking on fracture surfaces when the amount is small, and has been observed by others [14]. It may also be noted in the plot of crack depth vs. alloy, Fig. 14b, that in unirradiated samples, the maximum observed crack depth is always less than the irradiation depth (shown by the dashed line). However, irradiation to 7 dpa at either 400 °C or 500 °C results in crack depths that exceed the irradiated depth. Since the volume of material below the ion depth is unirradiated, the effect of irradiation on crack depth is only meaningful up to the ion penetration depth.

For the most part, cracking at 500 °C is more severe than that at 400 °C. The exceptions are the crack length per unit area and %IG

Table 5
Summary of cracking measurements from CERT experiments in SCW.

Temp (°C)	Alloy	Dose (dpa)	Strain (%)	Crack measurements Top values: unirradiated, bottom values: irradiated					
				%IG on fracture surface	Crack density (mm^{-2})	Max. crack depth (μm)	Avg. crack length (μm)	Crack length per unit area (μm/mm^2)	Norm. crack length per unit area (μm/mm^2/%strain)
400	316L	2	17	NM	102	NM	19	1969	116
				NM	129	NM	44	5712	336
			29[a]	0	173	12	27	4613	159
				24	110	32	60	6631	229
	316L	4	33[a]	0	166	9	36	5955	180
				69	130	38	54	6997	212
	316L	7	31[a]	0	158	6	35	5526	178
				100	134	37	56	7275	235
	690	2	17	NM	0	NM	0	0	0
				NM	7	NM	16	109	6
			46[a]	0	7	6	20	147	3
				6	38	14	35	1346	29
	690	4	17	NM	0	NM	0	0	0
				NM	10	NM	15	138	8
			56[a]	0	6	11	25	149	3
				7	44	16	35	1548	28
	690	7	17	NM	0	NM	0	0	0
				NM	13	NM	19	247	15
			46[a]	0	8	6	22	186	4
				9	48	18	34	1671	36
500	D9	7	12[a]	0	0	0	0	0	0
				26	22	22	19	425	35
	316L	7	19	NM	18	NM	31	569	30
				NM	32	NM	39	1254	66
			26[a]	0	19	8	30	578	22
				38	48	48	39	1905	73
	690	7	20	NM	8	NM	24	198	10
				NM	131	NM	62	8086	404
			27[a]	0	21	8	20	424	16
				100	153	51	55	8426	312
	800H	7	19	NM	0	NM	0	0	0
				NM	8	NM	86	658	35
			39[a]	0	1	12	89	97	2
				28	14	47	145	2070	53

NM = not measured.
[a] Failure strain.

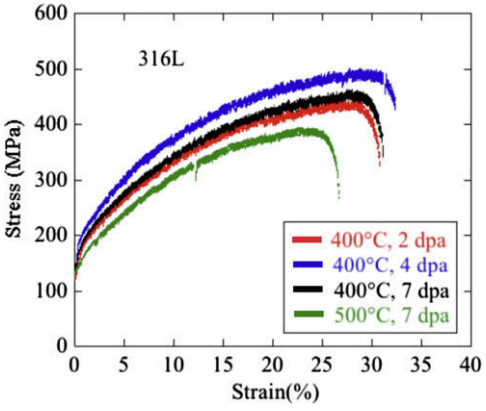

Fig. 11. Stress–strain behavior of 316L irradiated to 2, 4 and 7 dpa at 400 °C and to 7 dpa at 500 °C and tested in SCW at the same temperature at a strain rate of $3 \times 10^{-7}\ s^{-1}$.

for 316L in which the cracking at 400 °C is more severe. This behavior is puzzling but is consistent between the irradiated and unirradiated case indicating that in this alloy, cracking is more severe at 400 °C than at 500 °C. An earlier study [4] also found that cracking in 316L as measured by crack length per unit area in 316L was greater at 400 °C than at 500 °C.

4.2. Hardness and microstructure

Hardening has been cited as a key factor in IASCC susceptibility [15]. The cracking severity for 316L and 690 as measure by normalized crack length per unit area is plotted as a function of the measured change in hardness in Fig. 18. For 316L, the cracking increases with hardness, irrespective of irradiation and testing temperature. Cracking is more severe at 400 °C than at 500 °C as noted earlier, but the slopes for the 400 and 500 °C data are similar. Alloys D9 and 800H also show increased cracking severity with hardness for irradiation and testing at 500 °C. The slopes are also similar to that for 316L though the severity is less. Although the hardness of as-received D9 is greater than that for 316L and 800H due to cold-working, the increase in hardening due to irradiation is similar to that for the other two alloys. This is likely due to the recovery of the cold-worked structure in D9 during irradiation at 500 °C.

The cracking behavior of 690 is more complicated than for 316L. Fig. 18 shows the correlation between cracking severity and hardness of alloy 690 at both 400 and 500 °C. It is interesting that at 400 °C, the slope of the correlation is similar (though a bit smaller) to that for 316L. However, the slope of the correlation at 500 °C is much greater than all of the other data sets. Since hardening generally results from the dislocation and void microstructure, the strengthening resulting from the measured microstructure was determined using Eqs. (1)–(3) for 316L and 690 and plotted in Fig. 19. While the data is sparse, it does indicate that for the most

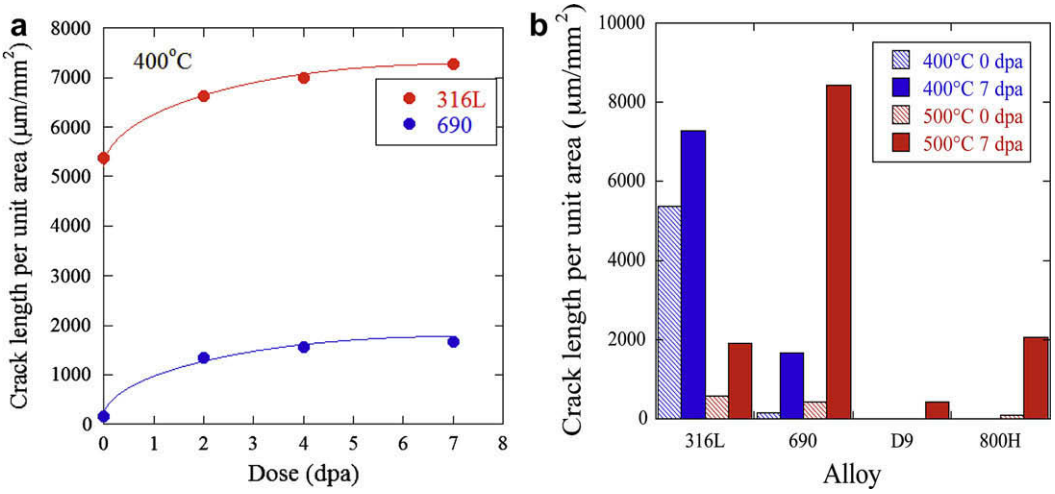

Fig. 12. Cracking severity as measured by crack length per unit area as a function of (a) dose at 400 °C and (b) alloy and temperature at 0 and 7 dpa.

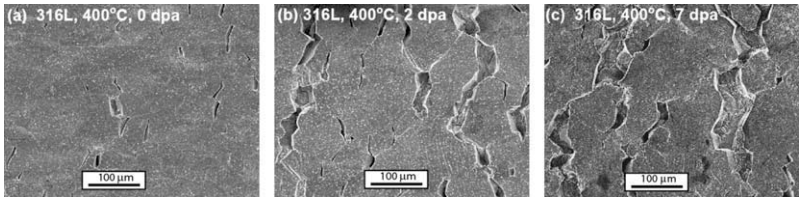

Fig. 13. Micrographs of gage surfaces of 316L specimens strained to failure in 400 °C SCW in the (a) unirradiated, (b) 2 dpa, and (c) 7 dpa conditions.

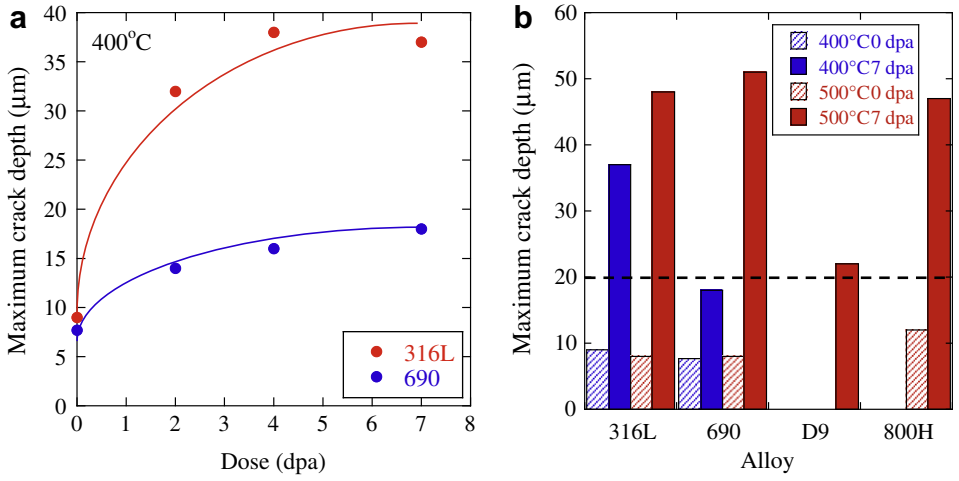

Fig. 14. Cracking severity as measured by maximum crack depth as a function of (a) dose at 400 °C and (b) alloy and temperature at 0 and 7 dpa. The dashed line indicates the depth of penetration of the 2 MeV protons.

part, the measured hardening can be accounted for by the loop and void microstructure. The 690 point with a yield stress determined from the microstructure of 624 MPa is from the 7 dpa, 400 °C irradiation. The 500 °C, 7 dpa irradiation that resulted in the severe IG cracking corresponds to the point with the lowest yield strength increase as determined from the loop and void microstructure. This analysis indicates that the irradiated microstructure and measured hardening are consistent with each other and neither explains the high amount of cracking in 690 after 7 dpa at 500 °C.

4.3. Radiation-induced segregation

Much data has been accumulated to support the role of chromium depletion as an agent in IGSCC of austenitic alloys in oxidizing conditions. The role of Cr as a beneficial element in iron-base austenitic alloys is well known. The presence of chromium increases the corrosion resistance through formation of a chromium-rich oxide, which passivates the alloy and leads to a reduction in the rate of general corrosion. Changes in grain

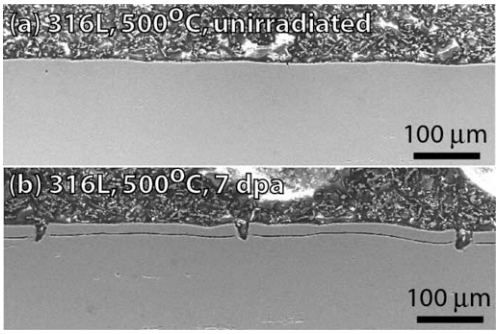

Fig. 15. Crack depths into (a) unirradiated and (b) 7 dpa surfaces of 316L specimens strained to failure in 500 °C SCW.

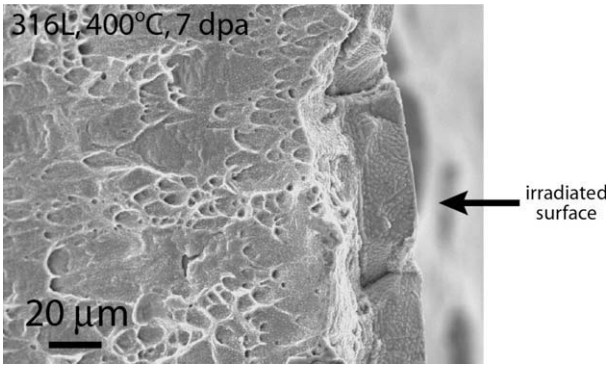

Fig. 17. Fracture surface of 316L strained to failure in 400 °C SCW following irradiation to 7 dpa at 400 °C. The irradiated portion of the specimen exhibited intergranular cracking, while the unirradiated portion of the specimen failed in a ductile manner.

boundary chemistry have been implicated in intergranular stress corrosion cracking (IGSCC) of unirradiated stainless steel and austenitic nickel-base [16] components for many years. The formation of chromium carbide ($Cr_{23}C_6$) precipitates at grain boundaries during heat treatment results in a local depletion of chromium in the regions surrounding the carbide, leaving the alloy in a sensitized state, which has been linked with cracking susceptibility in a number of studies [17–19]. Since RIS results in depletion of Cr at grain boundaries, analogous to that observed in thermally sensitized materials, irradiated alloys are also suspected to be susceptible to intergranular cracking. When the grain boundary chromium concentration drops below a critical level (typically about 17 wt.% for stainless steels [16]), passivation by formation of a protective chromium oxide over the grain boundary is no longer possible and the boundary becomes a location for oxide destabilization. As such, it has been generally accepted that radiation-induced segregation (RIS) is one of the most importance factors in IASCC [20–22].

Fig. 20 shows the correlation between the normalized crack length per unit area and the grain boundary Cr concentration for 316L and 690 irradiated and tested at 400 and 500 °C. In alloy 316L, the grain boundary Cr content decreases with dose (Fig. 14a), and as shown in Fig. 20, the grain boundary Cr concentration decreases from about 19 wt.% (0 dpa) to 11–12 wt.% after irradiation to 2 and 7 dpa. The cracking increases substantially from about 160 μm/mm²/%strain at 0 dpa to about 230 μm/mm²/%strain at 2 and 7 dpa. In this case, Cr segregation does not change much between 2 and 7 dpa and the cracking severity is also similar at each dose. At 500 °C, a similar dependence of cracking on dose is observed though the magnitude of cracking is considerably lower. In both cases, there is a significant increase in cracking severity with decreasing grain boundary Cr concentration.

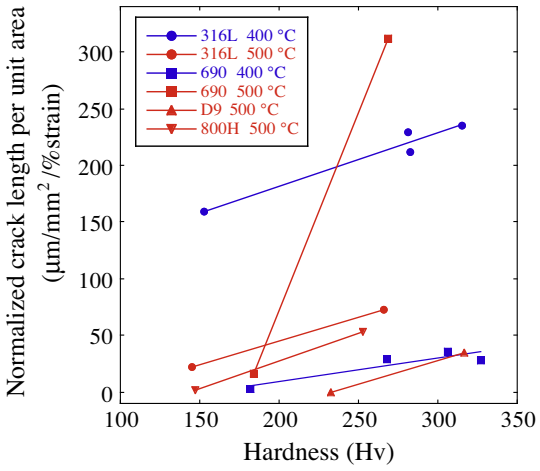

Fig. 18. Cracking severity as measured by normalized crack length per unit area vs. hardness for all alloys and temperatures.

The cracking behavior of alloy 690 with grain boundary Cr concentration is qualitatively similar to that for 316L, but there are

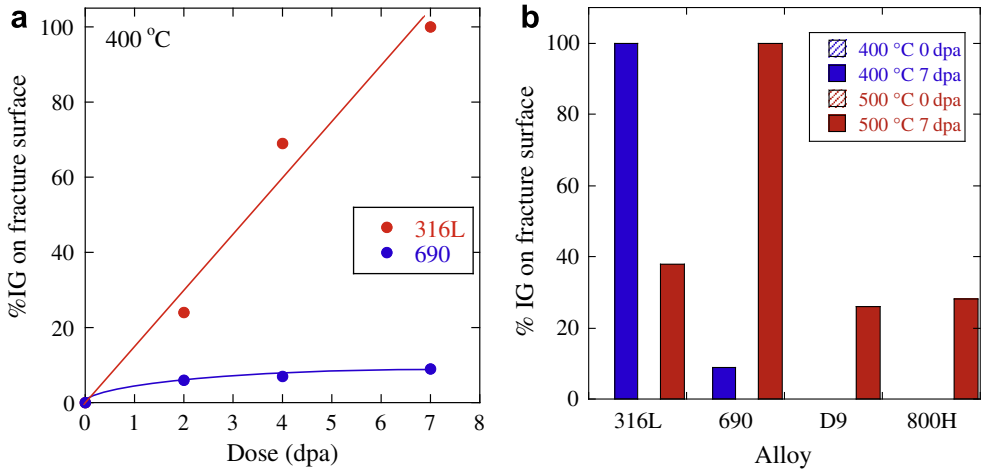

Fig. 16. Cracking severity as measured by %IG on the fracture surface as a function of (a) dose at 400 °C and (b) alloy and temperature at 0 and 7 dpa.

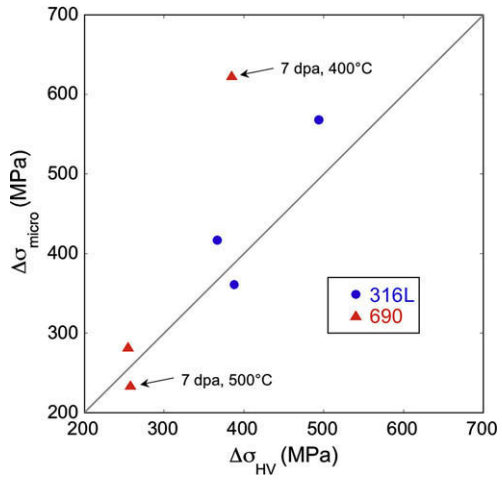

Fig. 19. Change in yield stress calculated from irradiation hardening vs. yield stress change calculated from irradiation microstructure for alloys 316L and 690.

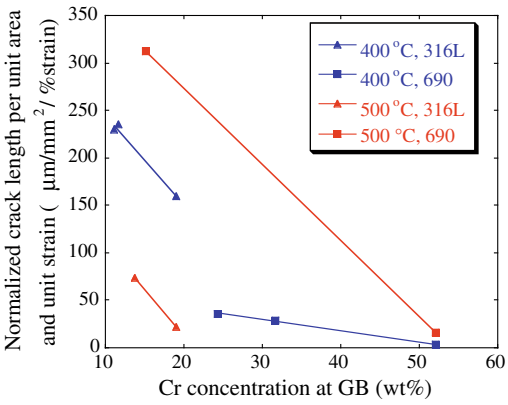

Fig. 20. Cracking severity as measured by normalized crack length per unit area vs. grain boundary Cr concentration for all alloys and temperatures.

some significant differences. First, as noted earlier, cracking is more severe at 500 °C than at 400 °C, which is opposite that in 316L. Second, the dependence of cracking on Cr content is very different at 400 vs. 500 °C. At 400 °C, cracking severity increases with decreasing grain boundary Cr content between 52% and 23% Cr. All of these Cr levels are above those required for passivity in this alloy and so despite the large change in grain boundary Cr content, a change in cracking severity is not expected. In fact, only the lowest grain boundary Cr concentration is below the bulk level as this heat had significant grain boundary Cr enrichment prior to irradiation and high irradiation dose was required to drop the level below that of the bulk. It is more likely that the increase in cracking severity is driven by the irradiation-induced hardening, which, as shown in Fig. 18 is modest but does correlate with cracking.

In contrast, at 500 °C the increase in cracking severity vs. grain boundary Cr is steeper and results in much greater cracking than for 316L at the same temperature. Unfortunately, there are only two data points for 690 at 500 °C and as just argued, it is unlikely that grain boundary Cr will affect cracking until the concentration is well below 20 wt.%, after which the amount of cracking would rise steeply to the value shown at 15% Cr. Given that all of the cracking vs. hardness correlations follow a consistent behavior with hardness except that for 690 at 500 °C, it is more likely that grain boundary Cr concentration was a factor in the cracking of 690 at 500 °C and 7 dpa.

Due to the difficulty in separating the components of the irradiated microstructure, attribution of cracking to a single irradiation-induced feature (hardening, RIS) is hard to support. Further, cracking may very well depend on other features not quantified here, such as the degree of localized deformation [23–24]. This situation is similar to cracking of irradiated alloys in subcritical water in which the mechanism has yet to be fully understood. However, the cracking behavior in supercritical water is very similar to that in subcritical water in that (1) any amount of irradiation enhances cracking severity, (2) cracking increases with irradiation dose, and (3) cracking generally increases with temperature [4]. It has also been noted that there is not a sharp disconnect in cracking of unirradiated alloys above and below the critical point, providing support for a common mechanism of cracking in both the sub- and supercritical water regimes.

5. Conclusions

- Alloys 316L and 690 exhibited susceptibility to IGSCC in both 400 °C and 500 °C SCW in the unirradiated condition. IGSCC at 500 °C is most severe in alloys 316L and 690, less severe in alloy 800H, and absent in D9.
- Irradiation increases the hardness of all alloys and the hardening at 400 °C is considerably greater than that at 500 °C. Hardening increases with dose at 400 °C, and at 500 °C, the hardening is greatest for alloys 316L and 800H and least for 690 and D9.
- Dislocation loops and voids are observed in both 316L and 690 at 400 °C and at 500 °C with loops dominating the irradiated microstructure in all cases. Increasing dose from 2 to 7 dpa at 400 °C results in a small increase in loop size for both alloys and an increase in the loop number density by factors of 2 to 4. Loop sizes are substantially larger and densities are lower at 500 °C vs. 400 °C. A similar behavior occurs for void size and number density.
- Both 316L and 690 in the as-received condition have significant grain boundary Cr enrichment. Irradiation of alloy 316L results in grain boundary Cr depletion for all doses, but only the highest dose at 400 and at 500 °C result in depletion of Cr below the bulk level in alloy 690.
- Irradiation results in increased cracking for all alloys regardless of dose or temperature. Cracking severity increases with dose and with temperature. The most severe cracking occurs in alloy 316L at 400 °C and 7 dpa, and in alloy 690 at 500 °C and 7 dpa.
- Cracking correlates with both increased hardening and decreased grain boundary chromium concentration. However, in the case of alloy 690 at 500 °C, grain boundary chromium appears to be the more important parameter. The cracking behavior of irradiated alloys in supercritical water follows the same trends as similar alloys in subcritical water.

Acknowledgements

Support for this project was provided by the U.S. Department of Energy under subaward A827761 of NERI grant DE-FC07-05ID14664. The authors are grateful to Ovidiu Toader and Fabian Naab of Michigan Ion Beam laboratory for the use of the irradiation facilities, and the Electron Microbeam Analysis Laboratory for the use of electron microscopes. A Portion of this research was conducted at the SHaRE User Facility, which is sponsored by the Division of Scientific User Facilities, Office of Basic Energy Sciences, U.S. Department of Energy.

References

[1] T.R. Allen, K. Sridharan, L. Tan, W.E. Windes, J.I. Cole, D.C. Crawford, G.S. Was, Nucl. Technol. 162 (2) (2008) 342–357.

[2] G.S. Was, P. Ampornrat, G. Gupta, J. Nucl. Mater. 371 (2007) 176.
[3] G. Gupta, G.S. Was, in: T.R. Allen, P.J. King, L.J. Nelson (Eds.), Proceedings of the 12th International Conference on Degradation of Materials in Nuclear Power Systems – Water Reactors, The Minerals, Metals and Materials Society, Warrendale, PA, 2005, pp. 1359–1368.
[4] S. Teysseyre, G.S. Was, Corrosion 62 (12) (2006) 1100–1116.
[5] G.S. Was, S. Teysseyre, Z. Jiao, Corrosion 62 (11) (2006) 989–1005.
[6] J.F. Ziegler, in: J.P. Biersack (Ed.), SRIM 2006, IBM Corporation, Yorktown, NY, 2006.
[7] Standard Practice for Neutron Radiation Damage Simulation of Charged-particle Irradiation, ASTM Designation E521-89, Annual Book of ASTM Standards, vol. 12.02, American Society for Testing and Materials, Philadelphia, PA, 1989, p. D-9.
[8] G. Gupta, Z. Jiao, A.N. Ham, J.T. Busby, G.S. Was, J. Nucl. Mater 351 (1–3) (2006) 162–173.
[9] J.T. Busby, M. Hash, G.S. Was, J. Nucl. Mater. 336 (2005) 267.
[10] G.S. Was, Fundamentals of Radiation Materials Science. Metals and Alloys, Springer, Berlin, 2007. p. 100.
[11] D.J. Edwards, E.P. Simonen, S.M. Bruemmer, J. Nucl. Mater. 317 (2003) 13.
[12] E.A. West, S. Teysseyre, Z. Jiao, G.S. Was, in: T.R. Allen, J. Busby, P.J. King (Eds.), Proceedings of the 13th International Conference on Degradation of Materials in Nuclear Power Systems – Water Reactors, Canadian Nuclear Society, Toronto, 2007.
[13] G.S. Was, P. Ampronrat, G. Gupta, S. Teysseyre, E.A. West, T.R. Allen, K. Sridharan, L. Tan, Y. Chen, X. Ren, C. Pister, J. Nucl. Mater. 371 (2007) 176–201.
[14] J.A. Begley, Strain-Rate Damage Model for Alloy 600 in Primary Water, Electric Power Research Institute, Report No. NP-7008s, 1990.
[15] G.S. Was, P.L. Andresen, Corrosion 63 (1) (2007) 19–45.
[16] S.M. Bruemmer, G.S. Was, J. Nucl. Mater. 216 (1994) 348.
[17] C.S. Tedmon Jr., J.A. Vermilyea, H.H. Rosolowski, J. Electrochem. Soc. 2 (1971) 192.
[18] S.M. Bruemmer, in: G.S. Was, S.M. Bruemmer (Eds.), Grain Boundary Chemistry and Intergranular Failure in Austenitic Stainless Steel, Mater. Sci. Forum., Trans Tech Publications, Switzerland, 1989, p. 309.
[19] S.M. Bruemmer, L.A. Charlot, Scr. Metall. 20 (7) (1986) 1019.
[20] S.M. Bruemmer, E.P. Simonen, P.M. Scott, Pl.L. Andresen, G.S. Was, J.L. Nelson, J. Nucl. Mater. 274 (1999) 299.
[21] P.M. Scott, J. Nucl. Mater. 211 (1994) 101.
[22] P.L. Andresen, Irradiation assisted stress corrosion cracking, in: R.H. Jones (Ed.), Stress Corrosion Cracking: Materials Performance and Evaluation, ASM International, 1992, pp. 181–210.
[23] Z. Jiao, G.S. Was, J. Nucl. Mater. 382 (2008) 203–209.
[24] G.S. Was, Z. Jiao, J.T. Busby, Proceedings of the International Symposium on Research for Aging Management of Light Water Reactors, Institute for Nuclear Safety Systems Inc., Fukui, Japan, 2007, pp. 8-1–8-23.